Title: Uniformitarian prediction of early-Pleistocene atmospheric CO_2

Authors and affiliations:
Parker Liautaud, Harvard University Department of Earth and Planetary Sciences
Peter Huybers, Harvard University Department of Earth and Planetary Sciences

Uniformitarian prediction of early-Pleistocene atmospheric CO_2

Parker Liautaud and Peter Huybers

Dept. of Earth and Planetary Sciences, Harvard University, Cambridge, MA, USA

May 15, 2022

Abstract

A number of groups attempted to predict atmospheric CO_2 concentrations between 420 to 800 ka prior to publication of the Dome C ice-core record by the European Project for Ice Coring in Antarctica, EPICA [44]. The predictions that fared best assumed that the relationships between CO_2 and proxies of air temperature remained consistent over the past 800 ky [7]. Here we extend predictions of atmospheric CO_2 concentrations over the last 2 Ma under a similar assumption of consistent physical relationships between CO_2 and climate over time and test this assumption against existing observations. Our principal approach is to use a recently-developed Bayesian paleoclimate model [25] to infer CO_2 values conditional on past sea level. An ensemble of seven different CO_2 histories are inferred from an equal number of sea-level reconstructions. Five of the ensemble members give a consensus prediction that CO_2 in the early Pleistocene, 2-0.8 Ma, averaged 241 ppm (238 ppm - 245 ppm 95% c.i.) with 95% of CO_2 values within 206 ppm and 275 ppm. Uncertainty estimates account for contributions from orbital forcing, the ice-albedo feedback, age uncertainties, and other factors.

The other two ensemble members indicate 20-50 meter higher sea level during the early Pleistocene and imply much higher CO_2 levels. Our consensus prediction aligns well with a compilation of previously published δ^{11}B-based CO_2 reconstructions that, after calibration to late-Pleistocene ice-core CO_2 values, average 237 ppm (95% of CO_2 values within 195 ppm to 273 ppm). Furthermore, 94% of consensus CO_2 predictions fall within the range indicated by 60 early-Pleistocene CO_2 measurements from air trapped in discontinuous ice segments from the Allan Hills in East Antarctica. Our consensus prediction can be definitively tested by obtaining continuous ice-core atmospheric CO_2 records that extend into the early Pleistocene.

1 Introduction

The first reconstructions of atmospheric composition over multiple glacial-interglacial cycles derived from the Vostok ice cores [2, 32] revealed a close relationship between atmospheric CO_2 and and global climate over at least the past 400,000 years. Atmospheric CO_2 decreased from ~280 ppm to ~180 ppm over order 100 ky periods before rising back to interglacial levels in order 10 ky, following the same sawtooth-like pattern that preceding studies had identified in the benthic δ^{18}O proxy for global ice-volume and deep-ocean temperature [18, 21]. The close coupling of CO_2 and ice volume gave crucial insight, albeit over a limited time interval, into the sensitivity of past climate. Importantly, a subsequent extension of the ice-core record to 650 ka [39] revealed that the relationship between CO_2 and δD, an air temperature proxy, remained consistent through at least 650 ka, and a similar finding was made when the ice-core record was eventually extended to 800 ka [28], its current extent.

The apparent stability of the CO_2-climate relationship might suggest we could predict CO_2 levels in earlier epochs on the basis of similar coupling, but it is unclear how similar the CO_2-climate relationships are before and after the mid-Pleistocene [11, 30, 35, 37]. Whereas late Pleistocene ice ages feature a strong ~100 ky component and follow a sawtooth pattern, their early-Pleistocene counterparts appear to mainly follow variations in obliquity at the 41-ky period [20, 33] and have smaller amplitude [38] and greater symmetry [1]. Specific evidence of changes over time in the CO_2-climate relationship comes from CO_2 reconstructions derived from foraminiferal Boron isotope ratios that indicate sea-level responded less sensitively to CO_2 radiative forcing in the early Pleistocene than in the late Pleistocene [10, 16].

There are several recent indications, however, that glacial-cycle characteristics did not change as much across the middle Pleistocene as previously described. In addition to obliquity-period variations, early-Pleistocene glacial cycles were shown to contain both significant climatic precession variability [24, 27] as well as $\sim$100 ky cycles [8, 13, 22, 26, 29], similar to the late Pleistocene.

In a previous study [25], we used a Bayesian approach to constrain a model of the relationships among orbital variations, CO_2, and sea-level. The model includes a zonally-averaged representation of an ice sheet that grows and retreats in response to orbital variations, CO_2 forcing, and meridional heat flux. We showed that observed changes in sea-level sensitivity to CO_2 forcing through the MPT [10] can be explained by ice-albedo feedbacks and nonlinear scaling of ice-sheet volume with length without requiring a change in dynamics over time. Here we build upon these results by conditioning the model upon seven different published sea-level reconstructions (Figure 1 and methods) in order to make a more-complete inference of early-Pleistocene CO_2 and comparing predictions against Boron isotope and old-ice indicators of early Pleistocene CO_2 levels. Two of the seven sea-level estimates are also accompanied by their own CO_2 inferences. The principle value of our analysis lies in providing a self-consistent set of data-constrained inferences of early-Pleistocene CO_2 for purposes of comparison to one another and against independent observations, and to make a specific prediction that can be tested by future observations.

2 Inverting sea level for early-Pleistocene CO_2

There are two broad patterns of Pleistocene sea-level variation among our seven different reconstructions, and they have diverging implications for the trajectory of Pleistocene CO_2 levels. According to one group of reconstructions – the first five displayed in Figure 1 – early-Pleistocene sea level varied with smaller amplitude than in the late Pleistocene. Glacials were milder with smaller ice sheets, but interglacials retained similar sea level as in the later interval. An alternative perspective [17, 34], suggests that interglacial sea-level was up to 20 – 50 meters higher during early-Pleistocene interglacials than in late-Pleistocene interglacials and implies a gradual trend toward overall colder average conditions as the Quaternary progressed. A similar pair of contrasting proposals has been put forward regarding the evolution of Pleistocene CO_2 levels, with some studies invoking a gradual trend toward lower average CO_2 [43], with consequent cooling of interglacials over the Pleistocene, and others suggesting only an intensification of glacials, with similar conditions across Pleistocene interglacials [10, 19, 45].

We take the five sea-level reconstructions with stable interglacial sea-level through the Pleistocene to represent a consensus reconstruction, and address them first. There is close agreement among the early-Pleistocene CO_2 values inferred from these five time series. The average inferred CO_2 between 2 and 1 Ma has a range across these models of just 5 ppm, from 241 ppm (239 ppm – 242 ppm) to 246 ppm (244 ppm – 248 ppm). Glacial-interglacial cycles also have similar amplitude across the five models: the 10th percentile of CO_2 levels ranges across models from 214 ppm (211 ppm – 216 ppm) to 217 ppm (214 ppm – 221 ppm), and the 90th percentile ranges from 264 ppm (261 ppm – 267 ppm) to 272 ppm (268 ppm – 277 ppm).

3 Comparison against δ^{11}B-derived CO_2 and Allan Hills blue-ice CO_2

Our consensus CO_2 prediction is compared against two sets of observational constraints. The first is a collection of 113 δ^{11}B-derived CO_2 estimates from [10], [19], and [16]. These data are used for their better agreement with late-Pleistocene ice core variations than many other biogeochemical proxies, such as those based on paleosols [14] or alkenones [36, 46], and because they contain two quasi-continuous segments in the early Pleistocene that span multiple glacial-interglacial cycles. The second constraint is a collection of 60 direct measurements of early Pleistocene CO_2 from discontinuous ice cores in the Allan Hills Blue Ice Area in East Antarctica. In keeping with our assumption that processes behave uniformly across the Pleistocene, we account for observational biases in both the δ^{11}B proxy and blue-ice CO_2 values under an assumption that factors affecting late-Pleistocene data proportionally affect early-Pleistocene data.

95% of inferred early-Pleistocene CO_2 values among the consensus predictions are between 206 ppm and 275 ppm (Figure 3a). As published, the δ^{11}B-based data indicate greater early-Pleistocene CO_2 variability (gray histogram in Figure 3b), ranging between 185 ppm (182 ppm – 200 ppm) and 319 ppm (307 ppm – 326 ppm), where the stated intervals represent 95% of values when resampling the data 10^4 times using the published uncertainties. Importantly, however, δ^{11}B-based CO_2 values also show greater variability during the late Pleistocene as compared against Antarctic ice-core CO_2 observations, suggesting that not all of the disagreement is from model error. Specifically, from 0 – 800 ka, the δ^{11}B-based CO_2 data give a mean value of 240 ppm and a range of 180 ppm, whereas ice-core values, which have much smaller uncertainty, give a mean of 224 ppm and a range of 125 ppm.

There are several factors that could lead to inferences from δ^{11}B overestimating CO_2 mean and variance, including a simplified representation of the relationship between pH and total alkalinity [10]. We scale the δ^{11}B CO_2 values over the last 2 Ma such by a factor that renders its range over last two glacial cycles, 10 – 260 ka, consistent with that of the composite ice-core record over that same time interval. After applying the late-Pleistocene derived adjustment, 95% of the δ^{11}B-derived data vary between 195 ppm (193 ppm – 204 ppm) and 273 ppm (266 ppm – 277 ppm) in the early Pleistocene, with an average of 237 ppm (blue histogram in Figure 3b). Consensus model ensemble values, similarly, have a 95% range of 206 to 275 and a mean of 241 ppm. Notwithstanding a remaining difference of 11 ppm in the lower 2.5th percentile, we note that the lowest model and δ^{11}B-derived CO_2 values are identical at 181 ppm. Accounting for the bias of the proxy data relative to late-Pleistocene ice cores is, apparently, sufficient to eliminate the majority of difference relative to early-Pleistocene consensus model estimates.

We next consider consistency of the consensus CO_2 prediction with the Allan Hills blue-ice data. One important question is the representativeness of a small number of blue-ice samples, particularly considering the fact that these observations are uncertain in age and concentrated in two depth sections that are 8 m and 22 m in length. We account for these factors by simulating the process of obtaining 60 clustered samples from our model ensemble. The average early- and mid-Pleistocene CO_2 value from these model samples is 241 ppm (221 ppm – 253 ppm), close to the blue-ice value of 239 ppm. The 2.5th and 97.5th percentiles of the 60 model values are respectively at 212 ppm (199 ppm – 230 ppm) and 268 ppm (249 ppm – 288 ppm), values that are statistically consistent with those from the observations at 217 ppm and 277 ppm. Green markers in Figure 3c indicate the mean, 2.5 percentile, and 97.5 percentile of the clustered samples from the model along with their 95% confidence intervals (Figure 3c).

A further important question is the role of temperature-dependence of ice accumulation rates. A random sample from an ice core in depth is more likely to recover an interglacial than a glacial sample because accumulation rates are generally higher during interglacials. For example, in the late Pleistocene [9] notes a doubling of accumulation rates from $\sim$2 cm yr^{-1} during glacials to $\sim$4 cm yr^{-1} during interglacials in the EPICA Dome C core. Similarly, [40] reports Holocene-LGM accumulation rate ratios of 1.8 at Vostok and 1.8-2.2 at Dome C, and [31] also identifies an approximate doubling in accumulation rates. It follows that a higher proportion of interglacial CO_2 values are expected to be present in the blue ice data relative to the true early-Pleistocene distribution of CO_2 values.

We repeat our sampling procedure after generating synthetic ice cores in which accumulation rates are sensitive to temperature. This further step leads to a subtle upward shift in the 2.5 and 97.5 model CO_2 percentiles, respectively to 217 ppm (202 ppm – 238 ppm) and 272 ppm (254 ppm – 289 ppm). This adjustment for variable accumulation rates thus gives a slight improvement in model agreement with the extremes of the blue-ice data (orange markers in Figure 3c). The adjustment also slightly increases the model average CO_2 to 248 ppm (236 ppm – 262 ppm), a value that remains consistent with the blue-ice average of 239 ppm.

4 Further discussion and conclusions

Two sea-level reconstructions [17, 34], are left out of the ensemble CO_2 estimate. Only a partial inference of CO_2 is possible from those records because they contain high sea levels that imply substantial Antarctic melting and are outside the domain of our Northern Hemisphere model. If we make a simple assumption that the interglacial relationship between CO_2 and sea-level holds at higher sea-levels, the reconstruction of Ref. 17 would imply early-Pleistocene CO_2 levels reaching 374 ppm and that of Ref. 34 would imply CO_2 levels reaching 479 ppm, a 50 – 200 ppm disagreement with the δ^{11}B-derived and blue-ice data. These results indicate that high early-Pleistocene sea-levels are unlikely to have occurred unless early-Pleistocene climate responded fundamentally differently to radiative forcing than late-Pleistocene climate.

Our results do not necessarily rule out more complicated explanations for observed early-Pleistocene CO_2 levels, including a role for regolith removal or changes in Antarctic ice-sheet stability that could imply consistency of high early-Pleistocene sea-level scenarios [17, 34] with CO_2 data. We propose, however, that these more-complicated mechanisms need not be invoked to explain presently available early-Pleistocene CO_2 data.

A main implication of our result is for the nature of the transition in glacial-cycle characteristics during the middle Pleistocene. The transition is widely suggested to arise from changes in the factors controlling ice-sheet responses to variations in radiative forcing, for example, through ice-sheet scouring of regolith in the Northern Hemisphere [12] or phase-locking of an internal climate mode to orbital forcing [41]. Our results instead suggest that the factors controlling the climate response remained consistent through the Pleistocene and that changes in the forcing associated with atmospheric CO_2 are instead responsible for changes in glaciation.

Our best estimate is that early-Pleistocene CO_2 varied between 206 ppm and 275 ppm (95% of values) and averaged 241 ppm, values derived from an assumption that processes controlling the relationship between sea level and CO_2 remained consistent throughout the Pleistocene. This prior assumption is well-supported by both bias-corrected reconstructions derived from foraminiferal δ^{11}B and direct air samples from ancient ice segments. The possibility of ice-core records that extend up to 1.5 My [5] and additional samples from the Allan Hills [23] suggest that a more complete test of these predictions may soon be possible.

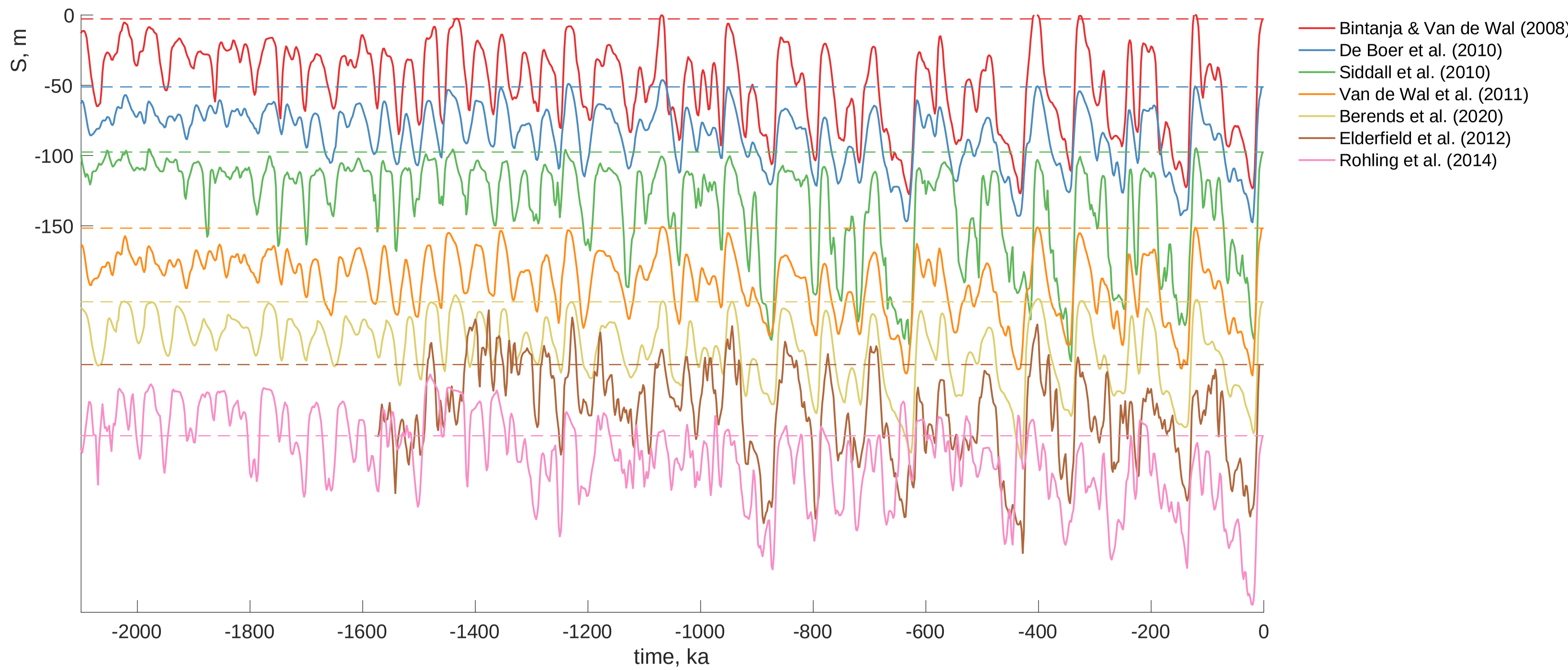

Figure 1: Seven sea-level reconstructions used in our inverse model to estimate atmospheric CO_2 levels through the Pleistocene. Only the estimates of Ref. 17 and Ref. 34 give sea-levels that are substantially higher than present day. Reconstructions are offset by 50m for visual clarity, and dotted lines indicate present-day sea level.

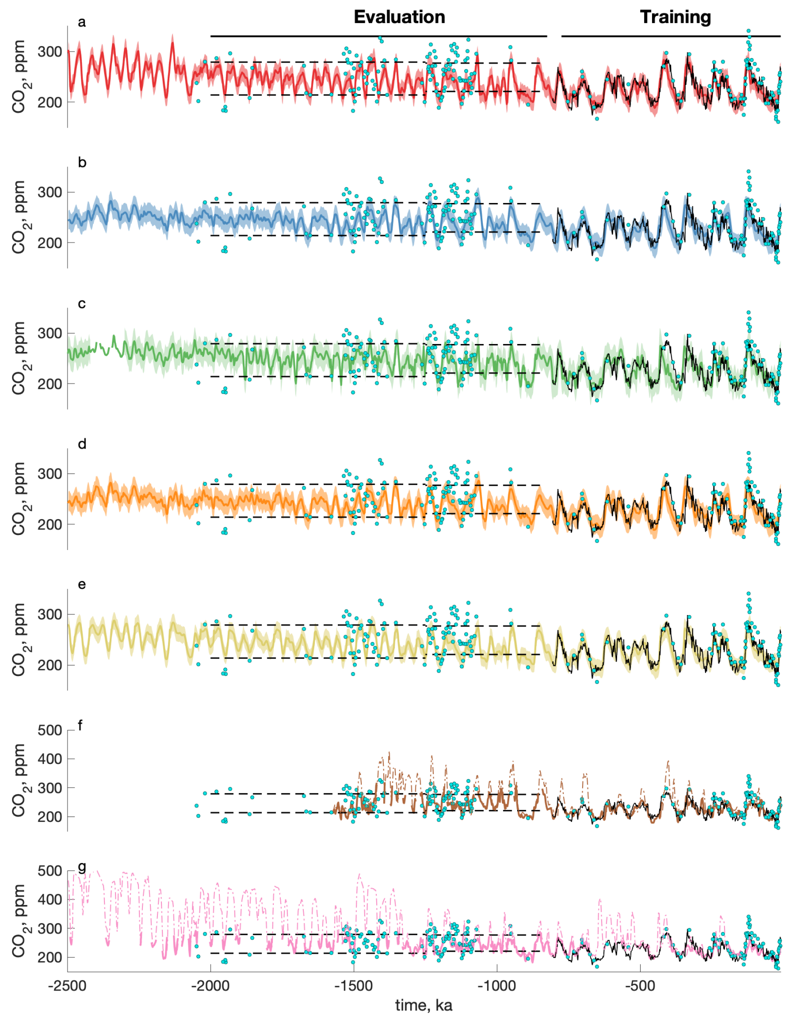

Figure 2: Inferred Pleistocene CO_2 values. Colors correspondwith Figure 1, and the 95% confidence intervals are indicated by the width of shading. The upper five reconstructions are broadly consistent among one another and generally agree with both δ^{11}B-derived reconstructions (blue markers) and the range of blue-ice measurements for the early and middle Pleistocene (black dashed lines). Note that δ^{11}B and blue-ice measurements are displayed here without calibration to the late-Pleistocene ice-core values. Sea levels more than 8m above present-day are outside the model domain, and where they occur in panels f and g we show an extrapolation based on linear regression of sea-level against CO_2 at values greater than 250 ppm (dash-dotted lines).

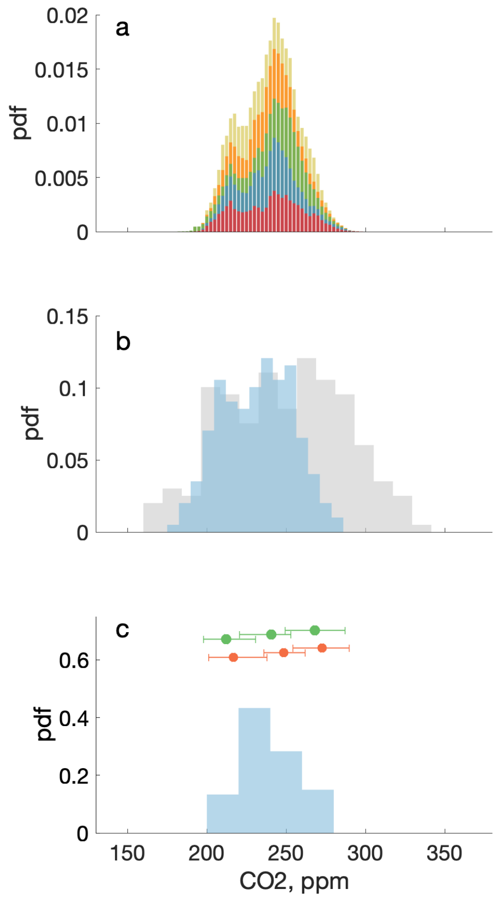

Figure 3: Consistency of multiple lines of evidence for early-Pleistocene CO_2 levels. **(a)** The distribution of model CO_2 inferred from a collection of five different sea-level reconstructions (stacked histogram). Colors correspond with those of the sea-level curves in Figure 1. **(b)** δ^{11}B-derived early-Pleistocene CO_2 reconstructions from Refs. 19, 10 and 16. Values are shown both as published (gray histogram) and after an adjustment to be consistent with late-Pleistocene ice-core CO_2 values (blue histogram). The adjustment brings δ^{11}B-derived values into close agreement with the model. **(c)** Agreement of the early Pleistocene blue-ice CO_2 values (blue histogram, $n = 60$) with the ensemble model results. The model and blue-ice data are consistent both if simulating clustered sampling of 60 values from the model ensemble (green markers, representing the 2.5th percentile, mean, and 97.5th percentile from left to right, and intervals representing their 95% c.i.) and if additionally accounting for the temperature-dependence of accumulation rates (orange markers and intervals, analogous to those in green).

Methods

Sea-level data

Ref. 34 converts δ^{18}O of planktonic foraminifera to relative sea level using a hydraulic model of the Mediterranean, the region from which the δ^{18}O record they use was obtained. Ref. 17 estimates the temperature component of benthic δ^{18}O on the basis of foraminiferal Mg/Ca ratios, and subtracts it from δ^{18}O to obtain an estimate of its ice-volume component. In Ref. 38 a piecewise-linear transfer function is developed for the relationship between δ^{18}O and global sea level by comparing a set of independent sea-level markers against coeval δ^{18}O levels, and linearly interpolating between the pairs of observations. δ^{18}O through the Pleistocene is converted to sea level under an assumption that this relationship remained stationary over the past 5 million years.

Whereas the reconstructions of Refs. 34, 17, and 38 exclusively use observational constraints, those of Refs. 6, 15, 42, and 4 use earth-system models to estimate the global ice-volume component of δ^{18}O. Ref. 6 models the effect of changes in atmospheric temperatures on ice volume using a three-dimensional ice-sheet model, and their effect on deep-water temperature using a simple linear scaling. Sea-level is reconstructed using an inverse approach in which changes in Northern Hemisphere air temperature implied by changes in δ^{18}O are propagated into the ice-sheet and deep ocean temperature models. Ref. 15 takes a similar approach but uses a one-dimensional ice sheet, and the methods of Refs. 42 and 4 are analagous to that of Ref. 6 but where implied changes in atmospheric CO_2 are additionally included in their model.

Bayesian sea-level and CO_2 model

Estimates of Pleistocene CO_2 conditional on sea level are obtained using the inverse model that is detailed in Ref. [25] and briefly summarized here. The relationship among orbital variations, atmospheric CO_2, and sea-level is represented using a zonally-averaged energy-balance balance model that is paired with an ice sheet following a plastic rheology. The model is inverted to estimate CO_2

levels as a function of the ice-sheet length that is implied by the input sea-level:

$$\varphi = \beta_0 + \beta_1 \frac{\mathrm{d}x_s}{\mathrm{d}t} \tag{1}$$

where $\varphi = \log([\mathrm{CO}_2]/278)$, x_s is the latitude of the southern terminus of the ice sheet. β_0 and β_1 are functions of eight physical parameters that include the ice-free and ice-covered surface albedos, temperature at which ablation overtakes accumulation, an outgoing longwave radiation parameter, the ice sheet sensitivity to ablation, the amplitudes of obliquity and climatic precession forcing, and the precession phase. β_0 and β_1 also depend on x_s and several specified constants such as the ice-sheet basal shear stress and upper terminus position of the ice sheet. Additionally, the relative ages of sea-level and CO_2 have important consequences for both implied orbital forcing and implied rates and magnitudes of the ice-sheet response to CO_2 changes. For this reason, sea-level and CO_2 ages are made flexible by interpolation between eight adjustable age-control points placed at every 100 ky in both time-series.

A joint posterior probability distribution for 8 physical parameters and 16 age parameters is obtained using a Bayesian sampling algorithm in which model-data error is assumed to follow a first-order autoregressive process for which the variance and degree of autocorrelation are inferred alongside model parameters. The inference procedure is repeated independently for each of the different sea-level reconstructions. To make an estimate of CO_2, parameters are drawn from the posterior distribution and used in combination with the sea-level curve in question to compute φ. A complete description of the model and inference procedure is in Ref. [25].

When sea-level is outside the model domain, the model returns no CO_2 value and those data are excluded in the Bayesian step to accept or reject a proposed set of parameters. Whereas it is necessary to retain a fixed number of data points through the algorithm, the presence of flexible ages in the algorithm means that the number of admissible data points may vary unpredictable with each parameter vector proposal. For this reason, when conducting inference using the sea-level records of [17] or [34], we use a fixed number of 340 admissible data points that, from manual tests, represents the maximum number feasible for our inversion strategy.

Comparison of ensemble model and blue-ice data

To evaluate consistency between model and blue-ice CO_2 values in the early and mid Pleistocene, we first generate synthetic ice cores in which accumulation rates can be made sensitive to temperature, then sample the synthetic cores using a method that accounts for clustering in the observations.

Generating synthetic cores with temperature-dependent accumulation rates

The accumulation rate, denoted A, increases with saturation vapor pressure, itself increasing exponentially with temperature [9]. Previous studies [3, 31] have used a simple parameterization for A based on changes in δD of the ice – a close proxy for local surface temperature – where $A = A_0 \exp(\beta \Delta D)$, A_0 is present-day accumulation rate, and β is an adjustable parameter. We adopt the similar parameterization $A = A_0 \exp(\gamma R_f)$, where γ is a constant and R_f is the CO_2 radiative forcing. A γ value of zero implies a constant accumulation rate, and we use this when neglecting temperature-dependent accumulation rates (green markers in Figure 3c). We otherwise use a value of $\gamma = 1.1$ (orange markers in Figure 3c) that is consistent with previous studies [9, 31, 40] in giving interglacial accumulation rates that are twice as high as glacial accumulation rates.

We neglect A_0 by setting it to 1 because it does not influence the relative probability of sampling from a glacial or interglacial within the same depth profile and because absolute depth plays no role in this test. In addition, the appropriate value of γ here is uncertain for several reasons, including that the parameterization for A is a simplification of a more complete expression that contains saturation vapor pressure and that the temperature-accumulation relationship is not spatially uniform but would depend on other factors, such as distance from the coast and height of the ice sheet.

Sampling the synthetic cores

The 60 blue-ice samples are distributed across two sections spanning 116m – 138m and 177m – 185m in depth. 82% of the samples are in the shallower section. Our synthetic sampling approach seeks to replicate both the observed clustering structure and sample fractions between the two sections. We randomly select two sections of the synthetic core, each having 1/20th the length of the core. 49 samples are randomly drawn without replacement from one section and, similarly, 11 samples are drawn from the other section. The process is repeated for each member of the posterior model ensemble, and the distribution of the resulting samples are then compared against that of the 60 blue-ice samples.

Extrapolation of CO_2 at high sea levels

Because the domain of our model extends only to 8 meters above present-day sea level, the sea-level reconstructions of Refs. 17 and 34 are too high throughout most of the early Pleistocene to yield a continuous CO_2 inference. For this reason we do not provide detailed CO_2 estimates from these reconstructions, but we undertake an extrapolation procedure to indicate the approximate range of CO_2 values they could imply. A linear regression is performed of CO_2 against sea level in late-Pleistocene interglacials, here defined as times when CO_2 exceeds 250 ppm. The regression relationship, having a slope of 1.1 m/ppm for both records, is used to extrapolate CO_2 when sea level is outside the model domain (dash-dotted lines in Figure 2). Over the 2-1 Ma interval of interest, extrapolated CO_2 reaches 384 ppm for the model based on [17] 479 ppm for the model based on [34].

References

[1] Y. Ashkenazy and E. Tziperman. Are the 41 kyr glacial oscillations a linear response to Milankovitch forcing? *Quaternary Science Reviews*, 23(18-19):1879–1890, 2004.

[2] J.-M. Barnola, P. Pimienta, D. Raynaud, and Y. S. Korotkevich. Co2-climate relationship as deduced from the vostok ice core: A re-examination based on new measurements and on a re-evaluation of the air dating. *Tellus B*, 43(2):83–90, 1991.

[3] L. Bazin, A. Landais, B. Lemieux-Dudon, H. T. M. Kele, D. Veres, F. Parrenin, P. Martinerie, C. Ritz, E. Capron, V. Lipenkov, et al. An optimized multi-proxy, multi-site Antarctic ice and gas orbital chronology (AICC2012): 120-800 ka. 2013.

[4] C. Berends, B. de Boer, and R. van de Wal. Reconstructing the Evolution of Ice Sheets, Sea Level and Atmospheric CO2 During the Past 3.6 Million Years. *Climate of the Past Discussions*, pages 1–22, 2020.

[5] T. Binder, N. Karlsson, and O. Eisen. First results from the Beyond EPICA-Oldest Ice pre-site survey in the Dome Fuji region, Antarctica. In *EGU General Assembly Conference Abstracts*, page 14050, 2017.

[6] R. Bintanja and R. van de Wal. North American ice-sheet dynamics and the onset of 100,000-year glacial cycles. *Nature*, 454(7206):869, 2008.

[7] E. J. Brook. Tiny bubbles tell all. *Science*, 310(5752):1285–1287, 2005.

[8] R. Caballero-Gill, T. Herbert, and H. Dowsett. 100-kyr Paced Climate Change in the Pliocene Warm Period, Southwest Pacific. *Paleoceanography and Paleoclimatology*, 34(4):524–545, 2019.

[9] A. Cauquoin, A. Landais, G. Raisbeck, J. Jouzel, L. Bazin, M. Kageyama, J.-Y. Peterschmitt, M. Werner, E. Bard, and A. Team. Comparing past accumulation rate reconstructions in East Antarctic ice cores using 10 Be, water isotopes and CMIP5-PMIP3 models. *Climate of the Past*, 11(3):355–367, 2015.

[10] T. Chalk, M. Hain, G. Foster, E. Rohling, P. Sexton, M. Badger, S. Cherry, A. Hasenfratz, G. Haug, S. Jaccard, et al. Causes of ice age intensification across the Mid-Pleistocene Transition. *Proceedings of the National Academy of Sciences*, 114(50):13114–13119, 2017.

[11] P. Clark, D. Archer, D. Pollard, J. Blum, J. Rial, V. Brovkin, A. Mix, N. Pisias, and M. Roy. The middle Pleistocene transition: characteristics, mechanisms, and implications for long-term changes in atmospheric pCO2. *Quaternary Science Reviews*, 25(23-24):3150–3184, 2006.

[12] P. Clark and D. Pollard. Origin of the middle Pleistocene transition by ice sheet erosion of regolith. *Paleoceanography and Paleoclimatology*, 13(1):1–9, 1998.

[13] S. Clemens and R. Tiedemann. Eccentricity forcing of Pliocene–early Pleistocene climate revealed in a marine oxygen-isotope record. *Nature*, 385(6619):801, 1997.

[14] J. Da, Y. G. Zhang, G. Li, X. Meng, and J. Ji. Low CO2 levels of the entire Pleistocene epoch. *Nature Communications*, 10(1):1–9, 2019.

[15] B. De Boer, R. Van de Wal, R. Bintanja, L. Lourens, and E. Tuenter. Cenozoic global ice-volume and temperature simulations with 1-D ice-sheet models forced by benthic δ18O records. *Annals of Glaciology*, 51(55):23–33, 2010.

[16] K. Dyez, B. Hönisch, and G. Schmidt. Early Pleistocene obliquity-scale pCO2 variability at 1.5 million years ago. *Paleoceanography and Paleoclimatology*, 33(11):1270–1291, 2018.

[17] H. Elderfield, P. Ferretti, M. Greaves, S. Crowhurst, I. McCave, D. Hodell, and A. Piotrowski. Evolution of ocean temperature and ice volume through the mid-Pleistocene climate transition. *Science*, 337(6095):704–709, 2012.

[18] J. Hays, J. Imbrie, N. Shackleton, et al. Variations in the Earth's orbit: pacemaker of the ice ages. *Science*, 194(4270):1121–1132, 1976.

[19] B. Hönisch, N. G. Hemming, D. Archer, M. Siddall, and J. F. McManus. Atmospheric carbon dioxide concentration across the mid-Pleistocene transition. *Science*, 324(5934):1551–1554, 2009.

[20] P. Huybers. Glacial variability over the last two million years: an extended depth-derived agemodel, continuous obliquity pacing, and the Pleistocene progression. *Quaternary Science Reviews*, 26(1-2):37–55, 2007.

[21] J. Imbrie and J. Z. Imbrie. Modeling the climatic response to orbital variations. *Science*, 207(4434):943–953, 1980.

[22] J. Z. Imbrie, A. Imbrie-Moore, and L. Lisiecki. A phase-space model for Pleistocene ice volume. *Earth and Planetary Science Letters*, 307(1-2):94–102, 2011.

[23] A. Kurbatov, E. Brook, S. Campbell, H. Conway, N. Dunbar, J. Higgins, N. A. Iverson, L. Kehrl, W. McIntosh, N. Spaulding, et al. Allan Hills Pleistocene Ice Project (PIP). In *AGU Fall Meeting Abstracts*, volume 2016, pages PP31B–2272, 2016.

[24] P. Liautaud, D. Hodell, and P. Huybers. Detection of significant climatic precession variability in early Pleistocene glacial cycles. *Earth and Planetary Science Letters*, 536:116137, 2020.

[25] P. Liautaud and P. Huybers. Increased sea level sensitivity to co2 forcing across the middle pleistocene transition from ice-albedo and ice-volume nonlinearities. *Journal of Climate*, 34(24):9693–9709, 2021.

[26] L. Lisiecki. Links between eccentricity forcing and the 100,000-year glacial cycle. *Nature Geoscience*, 3(5):349, 2010.

[27] L. Lisiecki and M. Raymo. Plio–Pleistocene climate evolution: trends and transitions in glacial cycle dynamics. *Quaternary Science Reviews*, 26(1-2):56–69, 2007.

[28] D. Lüthi, M. Le Floch, B. Bereiter, T. Blunier, J.-M. Barnola, U. Siegenthaler, D. Raynaud, J. Jouzel, H. Fischer, K. Kawamura, et al. High-resolution carbon dioxide concentration record 650,000–800,000 years before present. *Nature*, 453(7193):379–382, 2008.

[29] S. Meyers and L. Hinnov. Northern Hemisphere glaciation and the evolution of Plio-Pleistocene climate noise. *Paleoceanography*, 25(3), 2010.

[30] N. Opdyke. Pacific Core V28-239 Late Pliocene to Latest Pleistocene. *Investigation of late Quaternary Paleoceanography and Paleoclimatology*, 145:449, 1976.

[31] F. Parrenin, G. Dreyfus, G. Durand, S. Fujita, O. Gagliardini, F. Gillet, J. Jouzel, K. Kawamura, N. Lhomme, V. Masson-Delmotte, et al. 1-D-ice flow modelling at EPICA Dome C and Dome Fuji, East Antarctica. *Climate of the Past*, 3(2):243–259, 2007.

[32] J.-R. Petit, J. Jouzel, D. Raynaud, N. Barkov, J.-M. Barnola, I. Basile, M. Bender, J. Chappellaz, M. Davis, G. Delaygue, et al. Climate and atmospheric history of the past 420,000 years from the Vostok ice core, Antarctica. *Nature*, 399(6735):429–436, 1999.

[33] M. Raymo, L. Lisiecki, and K. Nisancioglu. Plio-Pleistocene ice volume, Antarctic climate, and the global δ18O record. *Science*, 313(5786):492–495, 2006.

[34] E. Rohling, G. Foster, K. Grant, G. Marino, A. Roberts, M. Tamisiea, and F. Williams. Sea-level and deep-sea-temperature variability over the past 5.3 million years. *Nature*, 508(7497):477, 2014.

[35] W. Ruddiman, M. Raymo, D. Martinson, B. Clement, and J. Backman. Pleistocene evolution: Northern Hemisphere ice sheets and North Atlantic Ocean. *Paleoceanography and Paleoclimatology*, 4(4):353–412, 1989.

[36] O. Seki, G. Foster, D. N. Schmidt, A. Mackensen, K. Kawamura, and R. Pancost. Alkenone and boron-based Pliocene pCO2 records. *Earth and Planetary Science Letters*, 292(1-2):201–211, 2010.

[37] N. Shackleton and N. Opdyke. Oxygen isotope and palaeomagnetic evidence for early Northern Hemisphere glaciation. *Nature*, 270(5634):216, 1977.

[38] M. Siddall, B. Hönisch, C. Waelbroeck, and P. Huybers. Changes in deep Pacific temperature during the mid-Pleistocene transition and Quaternary. *Quaternary Science Reviews*, 29(1-2):170–181, 2010.

[39] U. Siegenthaler, T. Stocker, E. Monnin, D. Lüthi, J. Schwander, B. Stauffer, D. Raynaud, J.-M. Barnola, H. Fischer, V. Masson-Delmotte, et al. Stable carbon cycle–climate relationship during the late pleistocene. *Science*, 310(5752):1313–1317, 2005.

[40] M. Siegert. Glacial–interglacial variations in central east antarctic ice accumulation rates. *Quaternary Science Reviews*, 22(5-7):741–750, 2003.

[41] E. Tziperman, M. Raymo, P. Huybers, and C. Wunsch. Consequences of pacing the Pleistocene 100 kyr ice ages by nonlinear phase locking to Milankovitch forcing. *Paleoceanography and Paleoclimatology*, 21(4), 2006.

[42] R. Van de Wal, B. d. Boer, L. Lourens, P. Köhler, and R. Bintanja. Reconstruction of a continuous high-resolution CO2 record over the past 20 million years. *Climate of the Past*, 7(4):1459–1469, 2011.

[43] M. Willeit, A. Ganopolski, R. Calov, and V. Brovkin. Mid-Pleistocene transition in glacial cycles explained by declining CO2 and regolith removal. *Science Advances*, 5(4):eaav7337, 2019.

[44] E. Wolff, C. Kull, J. Chappellaz, H. Fischer, H. Miller, T. F. Stocker, A. J. Watson, B. Flower, F. Joos, P. Köhler, et al. Modeling past atmospheric co2: results of a challenge. *Eos, Transactions American Geophysical Union*, 86(38):341–345, 2005.

[45] Y. Yan, M. Bender, E. Brook, H. Clifford, P. Kemeny, A. Kurbatov, S. Mackay, P. Mayewski, J. Ng, J. Severinghaus, et al. Two-million-year-old snapshots of atmospheric gases from Antarctic ice. *Nature*, 574(7780):663–666, 2019.

[46] Y. G. Zhang, A. Pearson, A. Benthien, L. Dong, P. Huybers, X. Liu, and M. Pagani. Refin-

ing the alkenone-pCO2 method I: Lessons from the Quaternary glacial cycles. *Geochimica et Cosmochimica Acta*, 260:177–191, 2019.